



Quantum Hall states for Rydberg arrays with laser-assisted dipole-dipole interactions

Tian-Hua Yang ^{1,2,*}, Bao-Zong Wang,^{1,2,*} Xin-Chi Zhou ^{1,2} and Xiong-Jun Liu ^{1,2,3,4,†}

¹International Center for Quantum Materials and School of Physics, Peking University, Beijing 100871, China

²Collaborative Innovation Center of Quantum Matter, Beijing 100871, China

³International Quantum Academy, Shenzhen 518048, China

⁴CAS Center for Excellence in Topological Quantum Computation, University of Chinese Academy of Sciences, Beijing 100190, China



(Received 19 April 2022; accepted 28 July 2022; published 8 August 2022)

Rydberg atoms with dipole-dipole interactions provide intriguing platforms to explore exotic quantum many-body physics. Here we propose a mechanism dubbed *laser-assisted dipole-dipole interactions* to realize synthetic magnetic field for Rydberg atoms in a two-dimensional array configuration, which gives rise to the exotic bosonic topological states. In the presence of an external effective Zeeman splitting gradient, the dipole-dipole interaction between neighboring Rydberg atoms along the gradient direction is suppressed but can be assisted when Raman lights are applied to compensate the energy difference. With this scheme we generate a controllable uniform magnetic field for the complex spin-exchange coupling model, which can be mapped to hard-core bosons coupling to an external synthetic magnetic field. The highly tunable flat Chern bands of the hard-core bosons are then obtained and, moreover, the bosonic fractional quantum Hall states can be achieved with experimental feasibility. This Letter opens up an intriguing avenue for the realization of the highly sought-after bosonic topological orders using Rydberg atoms.

DOI: [10.1103/PhysRevA.106.L021101](https://doi.org/10.1103/PhysRevA.106.L021101)

Introduction. The two-dimensional (2D) electrons coupled to an external magnetic field in the perpendicular direction can fill into Landau levels, giving rise to the prominent quantum Hall (QH) effects [1,2], whose discovery opened up the extensive search for topological states of quantum matter [3–7]. Unlike the electrons which are fermions, no quantum Hall states are obtained for noninteracting bosons coupled to external magnetic field since the bosons are condensed to the ground state at zero temperature, rather than filling into an entire Landau band. To realize the QH phase for bosons necessitates strong repulsive interactions so that the Bose liquids become incompressible and the bosonic QH effects may be reached [8–14]. In comparison with fermionic counterparts, the bosonic integer and fractional QH states are all strongly correlated topological phases, being intrinsic [15,16] or symmetry-protected topological orders [17–19]. Important attempts at achieving the QH regime have been made in bosonic systems, such as rotating Bose-Einstein condensates [20], Hofstadter-Hubbard model [21], and interacting photons [22], whereas the feasibility of fully realizing such strongly correlated topological phases in experiment is hitherto elusive.

Recently, the exploration of novel correlated quantum states using Rydberg atoms attracted remarkable interests [23]. The Rydberg atoms can be arranged individually in array configuration through optical tweezers [24–26]. The highly excited internal states enable the long-range dipole-dipole interactions, which generate effective hopping couplings between Rydberg atoms at different sites [27,28]. Such configuration simulates the hard-core bosons in lattice and provides

versatile platforms to explore correlated bosonic quantum matter. Several important fundamental correlated phases have been observed in experiment, including quantum magnetism [29–32], the one-dimensional bosonic Su-Schrieffer-Heeger model [28], and 2D quantum spin liquid [33]. To further realize the bosonic QH phase with Rydberg arrays necessitates the generation of synthetic magnetic field which is associated with complex-valued dipole-dipole interactions. The synthetic gauge fields are the key ingredient to explore topological physics and have been actively studied theoretically and experimentally for ultracold atoms in optical lattices [34–48]. The synthetic magnetic fields were also proposed for dipolar atoms [49,50], and a density-dependent Peierls phase was recently realized for a small system with three Rydberg atoms [51], whereas to realize a uniform magnetic field with high tunability for Rydberg arrays is currently a challenging task. Being intrinsically strongly correlated quantum simulators, the Rydberg atom arrays with synthetic magnetic fields are of great interests.

In this Letter, we propose a mechanism dubbed the *laser-assisted dipole-dipole interaction* for realizing a tunable synthetic magnetic field for hard-core bosons simulated by Rydberg atoms in a 2D array configuration. The realized model is described by the Hamiltonian,

$$\begin{aligned}
 H = & \sum_{j_x, j_y} (J_x b_{j_x+1, j_y}^\dagger b_{j_x, j_y} + J_y e^{i\Phi_{j_x}} b_{j_x, j_y+1}^\dagger b_{j_x, j_y} + \text{H.c.}) \\
 & + \sum_{j_x, j_y} (J_{d_1} e^{i\Phi_{j_x}} b_{j_x+1, j_y+1}^\dagger b_{j_x, j_y} + \text{H.c.}) \\
 & + \sum_{j_x, j_y} (J_{d_2} e^{i\Phi_{j_x}} b_{j_x-1, j_y+1}^\dagger b_{j_x, j_y} + \text{H.c.}), \quad (1)
 \end{aligned}$$

*These authors contributed equally to the work.

†Corresponding author: xiongjunliu@pku.edu.cn

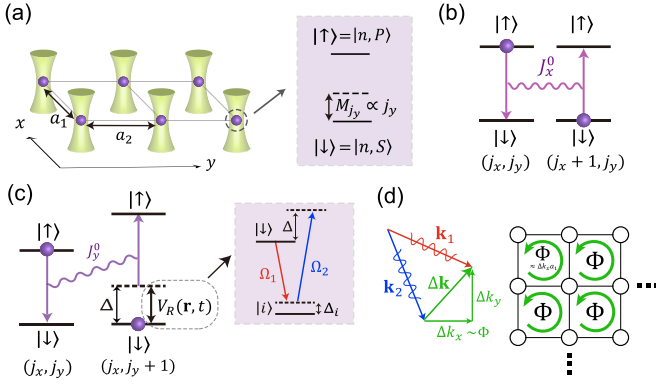


FIG. 1. Sketch of the proposal. (a) Rydberg atoms trapped in optical tweezers to form a 2D array. An energy shift with gradient in y direction modifies the energy difference between the two Rydberg states (effective Zeeman splitting for pseudospin). (b) The Rydberg dipole-dipole interaction can induce spin-exchange coupling between adjacent sites along the x direction. (c) In the y direction, the spin-exchange coupling is suppressed by the effective Zeeman energy offset. A two-photon Raman process compensates this energy offset and drives the laser-assisted spin-exchange couplings. (d) The laser-assisted exchange couplings have a spatially dependent phase, generating a synthetic magnetic flux in the 2D lattice.

where $b_{i,j}^\dagger$ ($b_{i,j}$) creates (annihilates) a hard-core boson at site (i, j) with particle number $\langle b_{i,j}^\dagger b_{i,j} \rangle \leq 1$, the coefficients $J_{x(y)}$ and $J_{d_1(d_2)}$ characterize the nearest-neighbor hopping term along the x (y) direction and next-nearest-neighbor (NNN) hopping terms in two diagonal directions, respectively. The hopping phase Φ represents a synthetic magnetic field for the hard-core bosons and is induced by the Raman laser-assisted dipole-dipole interactions. The flat Chern bands of the hard-core bosons are obtained with their flatness being drastically tuned by the diagonal J_{d_1, d_2} terms, facilitating the realization of bosonic QH states with Rydberg arrays.

The laser-assisted dipole-dipole interactions. We consider the 2D rectangular array of Rydberg atoms, with lattice constants $a_{1,2}$ and each trapped in optical tweezers [Fig. 1(a)]. Two Rydberg states are chosen to simulate spin 1/2 at each site with $|\downarrow\rangle \equiv |n, S\rangle$ and $|\uparrow\rangle \equiv |n, P\rangle$. An effective Zeeman splitting M_{j_y} between the two pseudospin states is introduced with $M_{j_y+1} - M_{j_y} = \Delta$ along the y direction, whereas the on-site energy along the x direction is uniform. The total Hamiltonian of the system,

$$H = H_{\text{dipole}} + H_{\text{Zeeman}} + V_R(\mathbf{r}, t) \quad (2)$$

includes the bare dipole-dipole interactions [23] which we take up to diagonal terms,

$$H_{\text{dipole}} = \sum_{j_x, j_y} (J_x^0 \sigma_{j_x, j_y}^+ \sigma_{j_x+1, j_y}^- + J_y^0 \sigma_{j_x, j_y}^+ \sigma_{j_x, j_y+1}^-) + \sum_{j_x, j_y} J_d^0 \sigma_{j_x, j_y}^+ \sigma_{j_x+1, j_y \pm 1}^- + \text{H.c.}, \quad (3)$$

the effective Zeeman energy gradient term,

$$H_{\text{Zeeman}} = \frac{1}{2} \sum_{j_x, j_y} M_{j_y} \sigma_{j_x, j_y}^z,$$

and the Raman coupling potential,

$$V_R(\mathbf{r}, t) = \frac{\Omega_1 \Omega_2^*}{\Delta_i} e^{i \Delta \mathbf{k} \cdot \mathbf{r}} e^{i(\omega_2 - \omega_1)t} \sigma_{j_x, j_y}^x + \text{H.c.}$$

In the above Hamiltonian, the dipole-dipole interaction leads to a spin-exchange coupling J_x^0 between adjacent sites along the x direction as illustrated in Fig. 1(b). The key ingredient of the scheme is that the bare exchange couplings J_y^0 and J_d^0 are suppressed by the relatively large Zeeman splitting offset Δ , but can be further induced by applying the Raman coupling potential V_R which is generated by two Raman lights with the Rabi-frequencies $\Omega_{1,2}$ and frequency difference $\omega_2 - \omega_1 \approx \Delta$ such that the Zeeman energy offset Δ is compensated by the two-photon process. Specifically, this Raman process is obtained by coupling one of the pseudospins to an intermediate state $|i\rangle$ with detuning Δ_i [see Fig. 1(c)]. With this configuration, the effective exchange couplings along the y and diagonal directions are recovered by the Raman laser-assisted dipole-dipole interactions. Furthermore, the wave-vector difference $\Delta \mathbf{k} = \mathbf{k}_2 - \mathbf{k}_1$ of two Raman lights determines the phases of the induced exchange couplings which are responsible to the magnetic flux in the effective model [Fig. 1(d)]. With the above analysis we can compute the effective exchange couplings through a time-dependent perturbation theory (see the Supplemental Material for details [52]),

$$J_y^{\text{eff}} = J_y^0 \frac{\Omega_1 \Omega_2^*}{\Delta \Delta_i} e^{i(\Phi_{j_x} + \phi_{j_y})} (e^{i\phi_y} - 1), \quad (4)$$

$$J_{d_1(d_2)}^{\text{eff}} = J_d^0 \frac{\Omega_1 \Omega_2^*}{\Delta \Delta_i} e^{i(\Phi_{j_x} + \phi_{j_y})} [e^{i[\phi_y + (-)\Phi]} - 1], \quad (5)$$

where $\Phi = \Delta k_x a_1$ is a nontrivial phase generating flux in each plaquette and the phase $\phi_y = \Delta k_y a_2$ tunes the strengths of J_y and $J_{d_1(d_2)}$. The term $e^{i\phi_y j_y}$ is, however, trivial and can be gauged out. We then reach the effective spin model in a more compact form

$$H_{\text{eff}} = \sum_{j_x, j_y} (J_x \sigma_{j_x+1, j_y}^+ \sigma_{j_x, j_y}^- + J_y e^{i\Phi_{j_x}} \sigma_{j_x, j_y+1}^+ \sigma_{j_x, j_y}^- + \text{H.c.}) + \sum_{j_x, j_y} (J_{d_1} e^{i\Phi_{j_x}} \sigma_{j_x+1, j_y+1}^+ \sigma_{j_x, j_y}^- + \text{H.c.}) + \sum_{j_x, j_y} (J_{d_2} e^{i\Phi_{j_x}} \sigma_{j_x-1, j_y+1}^+ \sigma_{j_x, j_y}^- + \text{H.c.}), \quad (6)$$

where J_{y, d_1, d_2} denote the amplitudes of the effective exchange couplings and $J_x = J_x^0$. The above model is mapped to the Hamiltonian (1) for hard-core bosons by defining the bosonic operator $b_j^\dagger = |\uparrow\rangle_j \langle\downarrow|_j$ at each site. Unlike the single-particle Raman process in optical lattices [36–39, 44–48], the present laser-assisted dipole-dipole interaction is a nonlinear two-particle process, rendering a strongly correlated bosonic system.

The Eq. (5) obtained in the perturbative regime is precise when Δ is large compared with the bare exchange couplings and the two-photon Raman coupling strength, namely, $J_{y, d}^0 / \Delta \ll 1$ and $|\Omega_1 \Omega_2^*| / (\Delta \Delta_i) \ll 1$. However, the generation of the magnetic flux through the laser-assisted dipole-dipole interactions is valid for more generic case beyond perturbative regime. The only difference is that for a

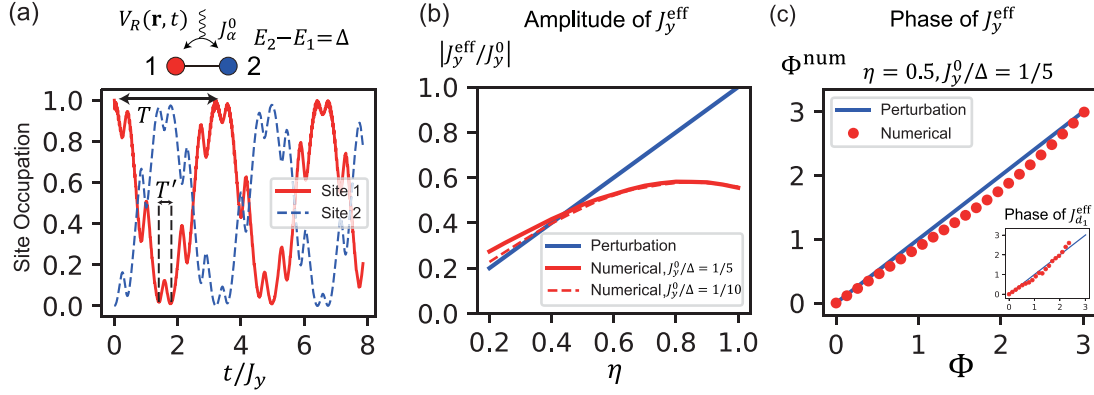


FIG. 2. Numerical simulation for the laser-assisted exchange couplings and the synthetic magnetic flux under $\phi_y = \pi$. (a) Raman coupling driven Rabi oscillation on a two-site system, which has an energy offset Δ compensated by the Raman potential. A boson is initialized at site 1 and evolves afterwards. Take $\eta = 2|\Omega_1\Omega_2/(\Delta\Delta_i)| = 0.5$ and $\Delta = 5J_y^0 = 10J_y$. The slow oscillation is driven by the Raman coupling, whereas the fast oscillations of frequency Δ correspond to the off-resonant bare transition. (b) The amplitude of J_y^{eff} matches well with the perturbative result $|J_y^{\text{eff}}| = \eta J_y^0$ when η and J_y^0/Δ are small. When η is large, $|J_y^{\text{eff}}|$ deviates clearly from the perturbative results. (c) The phase of the exchange-couplings J_y, J_{d_1} , and J_{d_2} (not shown in figure). The numerical results show good coincidence with perturbation results.

moderate Δ , higher-order processes and additional intermediate processes will also contribute to the effective exchange couplings, which quantitatively modify the amplitudes in Eq. (5) as we show below.

We confirm the above results numerically by studying the hopping dynamics for a single boson along the y direction or diagonal direction as shown in Fig. 2. We initialize the state of the single boson occupying site 1, and simulate the Rabi oscillations by computing the dynamical evolution between the two sites from the original Hamiltonian (2) with which we determine the numerical result of J_y^{eff} (the numerical study for $J_{d_1(d_2)}^{\text{eff}}$ is similar, see the Supplemental Material [52]). Figure 2(a) shows an example of the Rabi oscillations from which one can read off directly the amplitude of J_y^{eff} . From the phase accumulation in the wave-function evolution, one can determine the phase $\varphi(j_x)$ of the exchange-coupling coefficient for fixed j_x . Furthermore, the magnetic flux per plaquette, denoted as Φ^{num} , is given by $\Phi^{\text{num}} = \varphi(j_x = 1) - \varphi(j_x = 0)$ in two separate simulations for the two-site system along the y direction, respectively, at $j_x = 0$ and $j_x = 1$. Figures 2(b) and 2(c) shows the numerical results (blue solid lines) compared with the perturbation results given by Eq. (5) (red dashed lines). We find that for relatively small J_y^0/Δ and $|\Omega_1\Omega_2^*|/(\Delta\Delta_i)$, the numerical results of the amplitude of the laser-assisted exchange coupling $|J_y^{\text{eff}}|$ match better those given from the perturbation theory [Fig. 2(b)]. In comparison, the numerical results for the flux Φ^{num} matches well the perturbation results in more generic results [Fig. 2(c)]. With this we see that in the generic case the laser-assisted exchange couplings are induced, together with a nontrivial phase generating the magnetic flux in the effective model.

Before proceeding we provide estimates for the model parameters in the real experiment. For the ^{87}Rb atoms, for instance, we may take the primary quantum number $n \sim 50$ for the Rydberg states, which are of the lifetime $\tau \sim 100 \mu\text{s}$ at low temperature [53]. The lattice constants $a_{1,2}$ can be taken to be $10\text{--}20 \mu\text{m}$ for which the bare exchange coupling is about $J_{x,y}^0 \approx 1$ to 2 MHz. Accordingly, it is sufficient to

set the effective Zeeman splitting offset as $\Delta \approx 5.0\text{--}10$ MHz to suppress the bare exchange couplings along the y and diagonal directions. When a Raman coupling with strength $\Omega_1\Omega_2/\Delta_i \sim 0.25\Delta$ is applied, the effective coupling of magnitudes $J_y \sim 0.6$ to 1.0 MHz is induced through numerical calculation. As a key ingredient of the present scheme, the effective Zeeman splitting offset between neighboring sites can be realized with various approaches in the real experiment. For example, one can apply additional optical lights, which can be set together with the optical tweezer lights, to couple one of the two Rydberg states say $|\downarrow\rangle$ and the ground-state $5S$ for ^{87}Rb atoms (or other low-energy normal states), giving an AC Stark shift to the Rydberg state $|\downarrow\rangle$. Using the same optical tweezer technique one can readily control the light field strength on each array at different j_y sites to realize the required effective Zeeman splitting offset. Another direct approach is apply a magnetic field with spatial gradient along the y direction, which induces the real Zeeman energy splitting between the S and P Rydberg atoms. More details can be found in the Supplemental Material [52].

Flat Chern bands for the Rydberg states. We proceed to study the topological Chern band physics of the realized Hamiltonian (1), which exhibit exotic features. In particular, in the presence of the NNN hopping $J_{d_{1(2)}}$, the energy spectra versus the flux $\Phi = (p/q)2\pi$ (with p and q being mutually prime integers) exhibits distinct characters in comparison with the conventional Hofstadter butterfly which is symmetric with respect to both Φ and energy [54,55]. Specifically, here the energy spectra are generically asymmetric, showing a deformed Hofstadter butterfly diagram [Fig. 3(a)]. A novel result is that for the π -flux regime, the bulk is gapped with nonzero Chern number [Fig. 3(b)], in stark contrast to the conventional case without diagonal terms where the bulk is gapless [55]. Furthermore, for $q = 5$, an extremely flat lowest Chern band is obtained [Fig. 3(c)].

The intriguing feature is that the NNN hopping coefficients $J_{d_{1(2)}}$ can drastically change the flatness ratio between the band-gap E_{gap} and band-width W regarding the lowest Chern

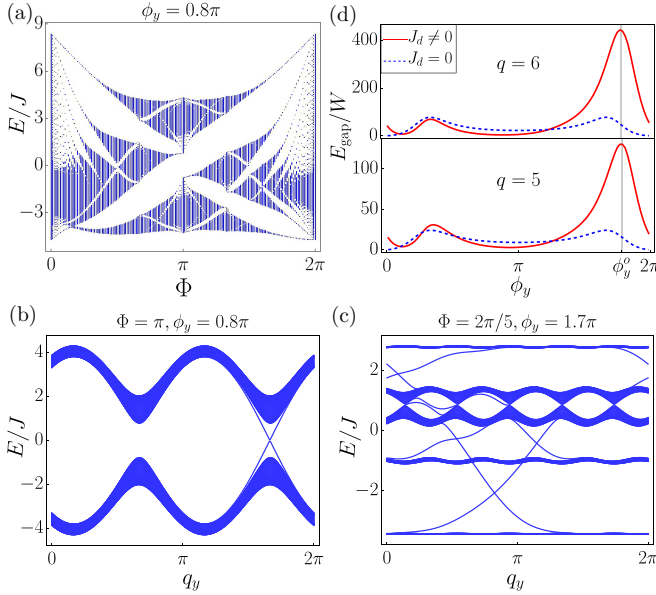


FIG. 3. The quantum Hall bands modulated by the diagonal hoppings $J_{d_1(d_2)}$ when $J_x^0 = J_y^0$. (a) The deformed Hofstadter butterfly is generated at $\phi_y = 0.8\pi$. (b) and (c) The Chern bands for different ϕ_y 's and Φ 's. (d) The flatness ratio E_{gap}/W versus ϕ_y . The red solid lines show the flatness ratio for the realized model in comparison with the case of setting $J_d = 0$ by hand (blue dashed line corresponding). The maximal flatness is obtained at $\phi_y = \phi_y^0$.

band. Figure 3(d) shows numerically the flatness ratio (the red solid lines) versus ϕ_y , which governs J_y and $J_{d_1(d_2)}$ via Eq. (5), and for comparison the flatness ratio for the case of setting $J_d = J_{d_{1,2}} = 0$ by hand is also given (the blue dashed lines). We find that the flatness of the lowest band is greatly improved in a large range of ϕ_y . Especially, at $\phi_y = \phi_y^0 \approx 1.7\pi$ with $J_x^0 = J_y^0 = 1$, the diagonal hoppings $J_{d_1} = 0.1e^{i0.55\pi}$ and $J_{d_2} = 0.6e^{i0.85\pi}$ for which the flatness ratio is optimized to maximum and is remarkably large. This feature enables a feasible way to realize bosonic fractional QH states.

Bosonic 1/2 Laughlin state. The flat Chern bands for hard-core bosons facilitate the realization of bosonic fractional QH states. In comparison with rotating Bose-Einstein condensates [14], the present Rydberg system realizes ideal Landau bands for hard-core bosons without necessitating the fast-rotating condition. Also, unlike the Hofstadter model for ultracold atoms in an optical lattice, the present model intrinsically reaches the strong interacting limit without suffering higher band effects. We denote the number of hard-core bosons as N_b and the filling factor $\nu = N_b/N_\varphi$, where N_φ is the total magnetic flux threading the 2D array. As a prominent example, we consider the filling $\nu = 1/2$, the ground many-body wave function of this bosonic Laughlin state reads [13,56]

$$\Psi_{\text{g.s.}}(z_1, \dots, z_{N_b}) = \prod_{j < k} (z_j - z_k)^2 \exp\left(-\sum_{i=1}^{N_b} |z_i|^2\right), \quad (7)$$

where $z_j = x_j + iy_j$ is the coordinate in the complex plane of the j th particle. The $\nu = 1/2$ fractional QH state is characterized by two fundamental features. First, the many-body ground states (g.s.s) have twofold degeneracy. Second, the

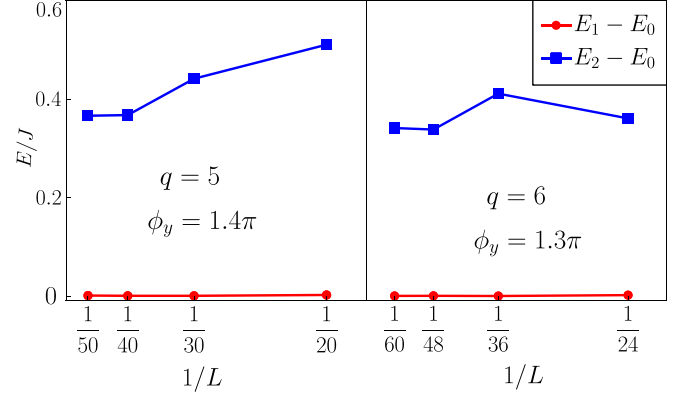


FIG. 4. The bosonic 1/2-fractional quantum Hall state. The low-energy spectra $E_n - E_0$ versus the system size $1/L$ with $L = L_x L_y$. The results show the twofold degeneracy of the many-body ground states, which have a finite gap separating from the excited states. Other parameters are taken $J_x = J_y = J$.

ground-state manifold is separated from excitations with a finite gap. Below we confirm the two features based on exact diagonalization for a finite system of $L_x L_y$ sites with periodic boundary condition.

The numerical results are shown in Fig. 4 where the hopping coefficients are set as $J_x = J_y = J$ for convenience at the phase $\phi_y = 1.4\pi$ (1.3π) for $q = 5$ (6). We compute the lowest three many-body eigenstates of the system with energies E_{0-2} and plot the spectra versus system size. We find the results are stabilized with sizes up to 5×10 for $q = 5$ and 6×10 for $q = 6$ at filling $\nu = 1/2$. The many-body ground states has twofold degeneracy as $E_1 - E_0 \approx 0$, whereas the excitation gap $E_{\text{gap}} = E_2 - E_1$ approaches an appreciable magnitude at large-size limit, yielding $E_{\text{gap}} = 0.37J$ for $q = 5$ and $E_{\text{gap}} = 0.35J$ for $q = 6$ for the present fractional QH phase. For both cases, the upper bound of correlation length can be estimated as $\xi_{\text{max}} \sim Ja/E_{\text{gap}} \sim 3a$, implying that the finite-size effects [69] are negligible for $L_{x,y} > 6a$ under the open boundary condition.

Conclusions and discussions. We have proposed a fundamental scheme dubbed the *laser-assisted dipole-dipole interactions* for Rydberg atoms to realize synthetic magnetic field and 2D bosonic QH states. The dipole-exchange interaction along one direction of the 2D Rydberg array is suppressed by setting an effective Zeeman splitting gradient but can be assisted by applying a two-photon Raman coupling process which compensates the neighboring-site Zeeman energy offset and generates nontrivial gauge flux for the spin-exchange model. The highly tunable flat Chern bands of hard-core bosons and the bosonic fractional QH states can be obtained feasibly, with the 1/2-Laughlin state being exemplified. Being a basic mechanism, the laser-assisted dipole-dipole interaction can be engineered and broadly applied to various Rydberg array configurations. For example, instead of externally controlling the energy-offset gradient of the Rydberg states, our scheme can also be applied to Rydberg superarrays consisting of different Rydberg atoms with intrinsic neighboring energy offsets. Thus, this mechanism can greatly expand the capability of engineering Rydberg atoms coupling to synthetic

gauge fields and may open an avenue to realize exotic correlated topological models and explore the highly sought-after bosonic topological orders with experimental feasibility.

Note added. Recently, we were notified that a recent preprint proposed a different interesting scheme to realize synthetic gauge fields for Rydberg atoms through coupling to multicolor lasers [70].

Acknowledgments. We thank S. Yu and Z.-X. Liu for fruitful discussions. This Letter was supported by National Key Research and Development Program of China (Grant No. 2021YFA1400900), the National Natural Science Foundation of China (Grants No. 11825401 and No. 11921005), and the Strategic Priority Research Program of Chinese Academy of Science (Grant No. XDB28000000).

-
- [1] K. V. Klitzing, G. Dorda, and M. Pepper, New Method for High-Accuracy Determination of the Fine-Structure Constant Based on Quantized Hall Resistance, *Phys. Rev. Lett.* **45**, 494 (1980).
- [2] D. C. Tsui, H. L. Stormer, and A. C. Gossard, Two-Dimensional Magnetotransport in the Extreme Quantum Limit, *Phys. Rev. Lett.* **48**, 1559 (1982).
- [3] M. Z. Hasan and C. L. Kane, Colloquium: Topological insulators, *Rev. Mod. Phys.* **82**, 3045 (2010).
- [4] X.-L. Qi and S.-C. Zhang, Topological insulators and superconductors, *Rev. Mod. Phys.* **83**, 1057 (2011).
- [5] B. Yan and S.-C. Zhang, Topological materials, *Rep. Prog. Phys.* **75**, 096501 (2012).
- [6] C.-K. Chiu, J. C. Y. Teo, A. P. Schnyder, and S. Ryu, Classification of topological quantum matter with symmetries, *Rev. Mod. Phys.* **88**, 035005 (2016).
- [7] B. Yan and C. Felser, Topological materials: Weyl semimetals, *Annu. Rev. Condens. Matter Phys.* **8**, 337 (2017).
- [8] N. K. Wilkin, J. M. F. Gunn, and R. A. Smith, Do Attractive Bosons Condense? *Phys. Rev. Lett.* **80**, 2265 (1998).
- [9] N. K. Wilkin and J. M. F. Gunn, Condensation of “Composite Bosons” in a Rotating BEC, *Phys. Rev. Lett.* **84**, 6 (2000).
- [10] B. Paredes, P. Fedichev, J. I. Cirac, and P. Zoller, $\frac{1}{2}$ -Anyons in Small Atomic Bose-Einstein Condensates, *Phys. Rev. Lett.* **87**, 010402 (2001).
- [11] N. R. Cooper, N. K. Wilkin, and J. M. F. Gunn, Quantum Phases of Vortices in Rotating Bose-Einstein Condensates, *Phys. Rev. Lett.* **87**, 120405 (2001).
- [12] T.-L. Ho, Bose-Einstein Condensates with Large Number of Vortices, *Phys. Rev. Lett.* **87**, 060403 (2001).
- [13] A. S. Sørensen, E. Demler, and M. D. Lukin, Fractional Quantum Hall States of Atoms in Optical Lattices, *Phys. Rev. Lett.* **94**, 086803 (2005).
- [14] Alexander L. Fetter, Rotating trapped bose-einstein condensates, *Rev. Mod. Phys.* **81**, 647 (2009)
- [15] X.-G. Wen, Topological orders and edge excitations in fractional quantum Hall states, *Adv. Phys.* **44**, 405 (1995).
- [16] X. Chen, Z.-C. Gu, and X.-G. Wen, Local unitary transformation, long-range quantum entanglement, wave function renormalization, and topological order, *Phys. Rev. B* **82**, 155138 (2010).
- [17] X. Chen, Z.-C. Gu, and X.-G. Wen, Symmetry protected topological orders and the group cohomology of their symmetry group, *Phys. Rev. B* **87**, 155114 (2013)
- [18] Y.-M. Lu and A. Vishwanath, Theory and classification of interacting integer topological phases in two dimensions: A Chern-Simons approach, *Phys. Rev. B* **86**, 125119 (2012).
- [19] T. Senthil and M. Levin, Integer Quantum Hall Effect for Bosons, *Phys. Rev. Lett.* **110**, 046801 (2013).
- [20] N. Gemelke, E. Sarajlic, and S. Chu, Rotating few-body atomic systems in the fractional quantum Hall regime, [arXiv:1007.2677](https://arxiv.org/abs/1007.2677).
- [21] M. E. Tai, A. Lukin, M. Rispoli, R. Schittko, T. Menke, D. Borgnia, P. M. Preiss, F. Grusdt, A. M. Kaufman, and M. Greiner, Microscopy of the interacting Harper Hofstadter model in the two-body limit, *Nature (London)* **546**, 519 (2017).
- [22] L. W. Clark, N. Schine, C. Baum, N. Jia, and J. Simon, Observation of Laughlin states made of light, *Nature (London)* **582**, 41 (2020).
- [23] A. Browaeys and T. Lahaye, Many-body physics with individually controlled Rydberg atoms, *Nat. Phys.* **16**, 132 (2020).
- [24] D. Barredo, S. de Léséleuc, V. Lienhard, T. Lahaye, and A. Browaeys, An atom-by-atom assembler of defect-free arbitrary two-dimensional atomic arrays, *Science* **354**, 1021 (2016).
- [25] M. Endres, H. Bernien, A. Keesling, H. Levine, E. R. Anschuetz, A. Krajenbrink, C. Senko, V. Vuletić, M. Greiner, and M. D. Lukin, Atom-by-atom assembly of defect-free one-dimensional cold atom arrays, *Science* **354**, 1024 (2016).
- [26] D. Barredo, V. Lienhard, S. de Léséleuc, T. Lahaye, and A. Browaeys, Synthetic three-dimensional atomic structures assembled atom by atom, *Nature (London)* **561**, 79 (2018).
- [27] S. de Léséleuc, V. Lienhard, P. Scholl, D. Barredo, S. Weber, N. Lang, H. P. Büchler, T. Lahaye, and A. Browaeys, Observation of a symmetry-protected topological phase of interacting bosons with Rydberg atoms, *Science* **365**, 775 (2019).
- [28] S. K. Kanungo, J. D. Whalen, Y. Lu, M. Yuan, S. Dasgupta, F. B. Dunning, K. R. A. Hazzard, and T. C. Killian, Realizing topological edge states with Rydberg-atom synthetic dimensions, *Nat. Commun.* **13**, 972 (2022).
- [29] H. Labuhn, D. Barredo, S. Ravets, S. Léséleuc, T. Macrì, T. Lahaye, and A. Browaeys, Tunable two-dimensional arrays of single Rydberg atoms for realizing quantum Ising models, *Nature (London)* **534**, 667 (2016).
- [30] H. Bernien, S. Schwartz, A. Keesling, H. Levine, A. Omran, H. Pichler, S. Choi, A. S. Zibrov, M. Endres, M. Greiner, V. Vuletić, and M. D. Lukin, Probing many-body dynamics on a 51-atom quantum simulator, *Nature (London)* **551**, 579 (2017).
- [31] P. Scholl, M. Schuler, H. J. Williams, A. A. Eberharter, D. Barredo, K.-N. Schymik, V. Lienhard, L.-P. Henry, T. C. Lang, T. Lahaye, A. M. Läuchli, and A. Browaeys, Quantum simulation of 2D antiferromagnets with hundreds of Rydberg atoms, *Nature (London)* **595**, 233 (2021).
- [32] S. Ebadi, T. T. Wang, H. Levine, A. Keesling, G. Semeghini, A. Omran, D. Bluvstein, R. Samajdar, H. Pichler, W. W. Ho, S. Choi, S. Sachdev, M. Greiner, V. Vuletić, and M. D. Lukin,

- Quantum phases of matter on a 256-atom programmable quantum simulator, *Nature (London)* **595**, 227 (2021).
- [33] G. Semeghini, H. Levine, A. Keesling, S. Ebadi, T. T. Wang, D. Bluvstein, R. Verresen, H. Pichler, M. Kalinowski, R. Samajdar, A. Omran, S. Sachdev, A. Vishwanath, M. Greiner, V. Vuletić, and M. D. Lukin, Probing topological spin liquids on a programmable quantum simulator, *Science* **374**, 1242 (2021).
- [34] D. Jaksch and P. Zoller, Creation of effective magnetic fields in optical lattices: The Hofstadter butterfly for cold neutral atoms, *New J. Phys.* **5**, 56 (2003).
- [35] J. Struck, C. Ölschläger, M. Weinberg, P. Hauke, J. Simonet, A. Eckardt, M. Lewenstein, K. Sengstock, and P. Windpassinger, Tunable Gauge Potential for Neutral and Spinless Particles in Driven Optical Lattices, *Phys. Rev. Lett.* **108**, 225304 (2012).
- [36] M. Aidelsburger, M. Atala, M. Lohse, J. T. Barreiro, B. Paredes, and I. Bloch, Realization of the Hofstadter Hamiltonian with Ultracold Atoms in Optical Lattices, *Phys. Rev. Lett.* **111**, 185301 (2013).
- [37] H. Miyake, G. A. Siviloglou, C. J. Kennedy, W. C. Burton, and W. Ketterle, Realizing the Harper Hamiltonian with Laser-Assisted Tunneling in Optical Lattices, *Phys. Rev. Lett.* **111**, 185302 (2013).
- [38] M. Aidelsburger, M. Lohse, C. Schweizer, M. Atala, J. Barreiro, S. Nascimbène, N. Cooper, I. Bloch, and N. Goldman, Measuring the Chern number of Hofstadter bands with ultracold bosonic atoms, *Nat. Phys.* **11**, 162 (2015).
- [39] X.-J. Liu, Z.-X. Liu, K. T. Law, V. W. Liu, and T. K. Ng, Chiral topological orders in an optical Raman lattice, *New J. Phys.* **18**, 035004 (2016).
- [40] B. K. Stuhl, H.-I. Lu, L. M. Ayccock, D. Genkina, and I. B. Spielman, Visualizing edge states with an atomic Bose gas in the quantum Hall regime, *Science* **349**, 1514 (2015).
- [41] B. Andrews and G. Möller, Stability of fractional Chern insulators in the effective continuum limit of Harper-Hofstadter bands with Chern number $|C| > 1$, *Phys. Rev. B* **97**, 035159 (2018).
- [42] G. Jotzu, M. Messer, R. Desbuquois, M. Lebrat, T. Uehlinger, D. Greif, and T. Esslinger, Experimental realization of the topological Haldane model with ultracold fermions, *Nature (London)* **515**, 237 (2014).
- [43] N. Goldman and J. Dalibard, Periodically Driven Quantum Systems: Effective Hamiltonians and Engineered Gauge Fields, *Phys. Rev. X* **4**, 031027 (2014).
- [44] X.-J. Liu, K. Law, and T. Ng, Realization of 2D Spin-Orbit Interaction and Exotic Topological Orders in Cold Atoms, *Phys. Rev. Lett.* **112**, 086401 (2014).
- [45] Z. Wu, L. Zhang, W. Sun, X.-T. Xu, B.-Z. Wang, S.-C. Ji, Y. Deng, S. Chen, X.-J. Liu, and J.-W. Pan, Realization of two-dimensional spin-orbit coupling for Bose-Einstein condensates, *Science* **354**, 83 (2016).
- [46] B. Song, L. Zhang, C. He, T. F. J. Poon, E. Hajiyev, S. Zhang, X.-J. Liu, and G.-B. Jo, Observation of symmetry-protected topological band with ultracold fermions, *Sci. Adv.* **4**, eaao4748 (2018).
- [47] Y.-H. Lu, B.-Z. Wang, and X.-J. Liu, Ideal Weyl semimetal with 3D spin-orbit coupled ultracold quantum gas, *Sci. Bull.* **65**, 2080 (2020).
- [48] Z.-Y. Wang, X.-C. Cheng, B.-Z. Wang, J.-Y. Zhang, Y.-H. Lu, C.-R. Yi, S. Niu, Y. Deng, X.-J. Liu, S. Chen, and J.-W. Pan, Realization of an ideal Weyl semimetal band in a quantum gas with 3D spin-orbit coupling, *Science* **372**, 271 (2021).
- [49] N. Y. Yao, C. R. Laumann, A. V. Gorshkov, S. D. Bennett, E. Demler, P. Zoller, and M. D. Lukin, Topological Flat Bands from Dipolar Spin Systems, *Phys. Rev. Lett.* **109**, 266804 (2012).
- [50] N. Y. Yao, A. V. Gorshkov, C. R. Laumann, A. M. Läuchli, J. Ye, and M. D. Lukin, Realizing Fractional Chern Insulators in Dipolar Spin Systems, *Phys. Rev. Lett.* **110**, 185302 (2013).
- [51] V. Lienhard *et al.*, Realization of a Density-Dependent Peierls Phase in a Synthetic, Spin-Orbit Coupled Rydberg System, *Phys. Rev. X* **10**, 021031 (2020).
- [52] See Supplemental Material at <http://link.aps.org/supplemental/10.1103/PhysRevA.106.L021101> for details of the: (i) time-dependent perturbation theory, (ii) experimental parameters, and (iii) numerical simulation of two-site dynamics, which includes Refs. [53,57–68].
- [53] I. I. Beterov, I. I. Ryabtsev, D. B. Tretyakov, and V. M. Entin, Quasiclassical calculations of blackbody-radiation-induced depopulation rates and effective lifetimes of Rydberg nS , nP , and nD alkali-metal atoms with $n \leq 80$, *Phys. Rev. A* **79**, 052504 (2009).
- [54] P. G. Harper, Single Band Motion of Conduction Electrons in a Uniform Magnetic Field, *Proc. Phys. Soc. London Sect. A* **68**, 874 (1955).
- [55] D. R. Hofstadter, Energy levels and wave functions of Bloch electrons in rational and irrational magnetic fields, *Phys. Rev. B* **14**, 2239 (1976).
- [56] V. Kalmeyer and R. B. Laughlin, Equivalence of the Resonating-Valence-Bond and Fractional Quantum Hall States, *Phys. Rev. Lett.* **59**, 2095 (1987).
- [57] D. Barredo, H. Labuhn, S. Ravets, T. Lahaye, A. Browaeys, and C. S. Adams, Coherent Excitation Transfer in a Spin Chain of Three Rydberg Atoms, *Phys. Rev. Lett.* **114**, 113002 (2015).
- [58] C. S. Adams, J. D. Pritchard, and J. P. Shaffer, Assembled arrays of Rydberg-interacting atoms, *J. Phys. B: At., Mol. Opt. Phys.* **53**, 012002 (2019).
- [59] L. Béguin, A. Vernier, R. Chicireanu, T. Lahaye, and A. Browaeys, Direct Measurement of the van der Waals Interaction between Two Rydberg Atoms, *Phys. Rev. Lett.* **110**, 263201 (2013).
- [60] T. F. Gallagher, *Rydberg Atoms*, Cambridge Monographs on Atomic, Molecular, and Chemical Physics, No. 3 (Cambridge University Press, Cambridge/New York, 1994).
- [61] A. Ramos, R. Cardman, and G. Raithel, Measurement of the hyperfine coupling constant for $nS_{1/2}$ Rydberg states of ^{85}Rb , *Phys. Rev. A* **100**, 062515 (2019).
- [62] R. Löw, H. Weimer, J. Nipper, J. B. Balewski, B. Butscher, H. P. Büchler, and T. Pfau, An experimental and theoretical guide to strongly interacting Rydberg gases, *J. Phys. B: At., Mol. Opt. Phys.* **45**, 113001 (2012).
- [63] J. Lampen, H. Nguyen, L. Li, P. R. Berman, and A. Kuzmich, Long-lived coherence between ground and Rydberg levels in a magic-wavelength lattice, *Phys. Rev. A* **98**, 033411 (2018).
- [64] E. Gomez, S. Aubin, L. A. Orozco, and G. D. Sprouse, Lifetime and hyperfine splitting measurements on the 7s and 6p levels in rubidium, *J. Opt. Soc. Am. B* **21**, 2058 (2004).
- [65] R. F. Gutterres, C. Amiot, A. Fioretti, C. Gabbanini, M. Mazzoni, and O. Dulieu, Determination of the $^{87}\text{Rb}5p$ state dipole matrix element and radiative lifetime from the photoas-

- sociation spectroscopy of the $\text{Rb}_2\text{O}_g^-(P_{3/2})$ long-range state, [Phys. Rev. A **66**, 024502 \(2002\)](#).
- [66] R. Song, J. Bai, Y. Jiao, J. Zhao, and S. Jia, Lifetime measurement of cesium atoms using a cold Rydberg gas, [Appl. Sci. **12**, 2713 \(2022\)](#).
- [67] D. J. Griffiths and D. F. Schroeter, *Introduction to Quantum Mechanics*, third ed. (Cambridge University Press, Cambridge/New York, 2018).
- [68] D. Steck, *Rubidium 87 D Line Data* (2003).
- [69] M. Gerster, M. Rizzi, P. Silvi, M. Dalmonte, and S. Montangero, Fractional quantum Hall effect in the interacting Hofstadter model via tensor networks, [Phys. Rev. B **96**, 195123 \(2017\)](#).
- [70] X. Wu, F. Yang, S. Yang, K. Mølmer, T. Pohl, M. K. Tey, and L. You, Synthesizing Gauge fields via Multicolor Dressing of Rydberg-Atom Arrays, [arXiv:2203.03994](#).